2021 43rd Annual International Conference of the
IEEE Engineering in Medicine & Biology Society (EMBC)
Oct 31 - Nov 4, 2021. Virtual Conference

Bone Tissue Scaffolds Designed With A Porosity Gradient Based On Triply Periodic Minimal Surfaces Using A Parametric Approach

Mariana S. Flores-Jiménez[1] and Rita Q. Fuentes-Aguilar[1]

***Abstract*— Recently, the interest in porous scaffolds design for cell culture has increased. Because of the curvotaxis property of the cells, they can respond to the curvature of the substrate in which they are seeded, like changing their morphology, despite that, curvature is little explored within scaffold design. What is more, for bone regeneration, the scaffold should ideally have a porosity gradient corresponding to the transition between compact and cancellous bone. Various studies have focused on finding the best geometry to mimic it, being the triple periodic minimum structures (TPMS) the most promising ones. However, as they are mathematically complex, researchers have approximated them with implicit equations, no longer respecting their minimum curvature when they vary the pore size, deforming the original geometry. This work proposed to approach the TPMS with parametric equations, finding an exact fundamental patch. In this way showing its potential to make customized structures with a porous gradient, thanks to the acquisition of a constant of variation. This generates a friendly user interface for the design of scaffolds. The work also presents a comparison with the implicit structures, remarking the benefits of using the parametric approach. Finally, it presents examples of 3D printed designs.**

I. Introduction

In the tissue engineering field, bone regeneration is one of the most studied tissues since it can be damaged by multiple causes, such as degenerative diseases, deep injuries or physical wear. The few resources to use transplant replacements, like autograft, have increased the urgency to manufacture a suitable scaffold to cultivate cells, with a specific geometry that promotes the growth of tissue, imitating the original bone anatomy [4]. However, to find the correct design is not a simple task and has limited the complete tissue reproduction, being one of the greatest area of opportunity to improve. To begin with, the creation of a porous scaffold should consider its curvature, since "curvotaxis" influences the behavior of cells during differentiation (adhesion, migration and changes in morphology). There are two types of curvature: "K" or Gaussian (intrinsic), and "H" or mean (extrinsic). In scaffolds with K>0, the fibers can compress the nucleus and may not trigger the osteogenic pathways. Concave pits (H<0) can increase migration compared with convex, but they induce a "lift-off" behavior, hindering the attachment. Hence, it is suggested that the scaffold should adopt a saddle-like shape (K<0, H=0) [5]. The geometry of the bone has interconnected pores following a gradient, starting with the compact bone (porosity of $\approx 10\%$, average diameter of 0.10 mm). The diameter grows as it approaches to the center, the trabeculae (porosity of $\approx 90\%$, 0.50 mm to 1mm) [14]. Several designs have been proposed, commonly by stacking fibers one onto another, forming quadrangular, triangular or hexagonal void spaces [6], [2], or by opening circular channels along a prismatic structure [3], however, these forms are still far from giving a faithful imitation of the aforementioned anatomy. Some researches begin to focus on the Triple Periodic Minimum Surfaces (TPMS), which have local minimal area and no self-intersections. TPMS are symmetric and periodic in three independent directions, having H=0 and $K < 0$. The principal ones are the Diamond (D), the Primitive (P) and the Gyroid (G) [8]. TPMS have been tested in regenerative medicine, finding that cell proliferation in a G type scaffold incremented in comparison with rectangular geometries, showing a 10-times greater permeability [11]. However, TPMS have been modeled using an implicit equation, approximated by a nodal sum in terms of Fourier series [7]. This approach may be sufficient for a general design of TPMS (porosity of 50%), but, as the pore size is varied, the shape deforms, until it loses the properties of minimal curvature. Furthermore, the meshing of implicit surfaces for mechanical studies can be time-consuming and can cause errors in finite element simulations. The major contribution of this work is to parameterize the three main TPMS (D, P and G) using the Weierstrass equations. It is proposed a method to vary their porosity in order to design a customized gradient with smooth transitions, close to the bone anatomy. It is also shown a comparison between the implicit and parametric approaches and an example of 3D printed parametric structures is presented.

II. Methodology

This section describes the algorithm to parametrize the TPMS by solving the Weierstrass equations and obtaining a fundamental patch from which the entire surface can be generated by symmetry operations. Then, it is presented the procedure to find the constant for size variation along with the methodology to design a porous gradient scaffold. The procedures were performed in MATLAB 2019a ®.

A. The Weierstrass parameterization

For minimal surfaces, Weierstrass showed that the coordinates can be defined by a set of integrals in terms of a complex number $\omega = u + iv$ [8]. The integrals were treated as elliptic integrals; incomplete (F) and complete (K), and expressed in terms of the *Jacobi's and Legendre's form*. Using $a = 1$ as the unitarian bounding cell, and κ as

[1]School of Engineering and Sciences, Tecnológico de Monterrey, Zapopan, Jalisco, México ORCID 0000-0002-1392-7660, ORCID 0000-0003-2559-539X

"the normalization factor", the parametric equations for each TPMS are:

For D, with $\kappa = \frac{2a}{ellipticK(1/4)}$:

$$\begin{cases} x = \kappa Re\left(\frac{1}{2\sqrt{2}} ellipticF\left[arcsin\left(\frac{2\sqrt{2}\omega}{\sqrt{\omega^4+4\omega^2+1}}\right), \frac{1}{4}\right]\right) \\ y = \kappa Im\left(\frac{1}{2\sqrt{2}} ellipticF\left[arcsin\left(\frac{-2\sqrt{2}\omega}{\sqrt{\omega^4+4\omega^2+1}}\right), \frac{3}{4}\right]\right) \\ z = \kappa Re\left(\frac{1}{4} ellipticF\left[arcsin\left(\frac{4\omega^2}{\omega^4+1}\right), 97-56\sqrt{3}\right]\right) \end{cases} \quad (1)$$

For P, with $\kappa = \frac{2a}{ellipticK(3/4)}$:

$$\begin{cases} x = -\kappa Im\left(\frac{1}{2\sqrt{2}} ellipticF\left[arcsin\left(\frac{2\sqrt{2}\omega}{\sqrt{\omega^4+4\omega^2+1}}\right), \frac{1}{4}\right]\right) \\ y = \kappa Re\left(\frac{1}{2\sqrt{2}} ellipticF\left[arcsin\left(\frac{-2\sqrt{2}\omega}{\sqrt{\omega^4+4\omega^2+1}}\right), \frac{3}{4}\right]\right) \\ z = -\kappa Im\left(\frac{1}{4} ellipticF\left[arcsin\left(\frac{4\omega^2}{\omega^4+1}\right), 97-56\sqrt{3}\right]\right) \end{cases} \quad (2)$$

For G, with $K = ellipticK(1/4)$, $K' = ellipticK(3/4)$, $K'' = K^2 + K'^2$, $\kappa = a\sqrt{K''}/KK'$ and $\theta = arccot[K'/K] \approx 38.014º$:

$$\begin{cases} x = \kappa e^{i\theta} Re\left(\frac{1}{2\sqrt{2}} ellipticF\left[arcsin\left(\frac{2\sqrt{2}\omega}{\sqrt{\omega^4+4\omega^2+1}}\right), \frac{1}{4}\right]\right) \\ y = \kappa e^{i\theta} Im\left(\frac{1}{2\sqrt{2}} ellipticF\left[arcsin\left(\frac{-2\sqrt{2}\omega}{\sqrt{\omega^4+4\omega^2+1}}\right), \frac{3}{4}\right]\right) \\ z = \kappa e^{i\theta} Re\left(\frac{1}{4} ellipticF\left[arcsin\left(\frac{4\omega^2}{\omega^4+1}\right), 97-56\sqrt{3}\right]\right) \end{cases} \quad (3)$$

B. The fundamental patch

Equations (1) to (3), were evaluated in the specific domain for each surface, within the complex plane, as indicated in [8]. Once the fundamental patch (FP) was generated, the complete structure was formed, first by obtaining a "bounding cell" (BC) (joining 6 FP for the D and P, and 12 for the G), then by generating a "cubic cell" (CC) (using 4 BC for the D surface, and 8 for the P and G). The process of joining the surfaces were achieved following the symmetry operations indicated in [8], [9], [10].

C. TPMS pore size variation

Parametric equations (1)-(3) are defined for surfaces with a specific surface-to-volume ratio of 50%, therefore, there is not an exact equation to find their *constant minimal companions* (CMC). This work aims to solve this problem by a manipulation of the normal vectors, with the next steps:

- Obtain the normal vectors (NV) of each point on the FP.
- Define a variable δ to indicate the pore size variation.
- Define an offset value, multiplying δ by NV.
- Add the offset value to the original coordinates.
- For the P surface, proceed to symmetry operations. For the G, for the first two BC, δ should be positive, and for the next two, δ should be negative, and so on. For D, first BC should be positive, next one negative and so on.

To control the pore size, a constant of variation was obtained, first by measuring the surface strut and the pore size along the diagonal of the CC, then by using a polynomial fit to obtain the relationship between δ and the porosity measured, based on [12].

D. Porosity gradient with TPMS

The smooth gradient was achieved without using any step function, since the exact points of each CC were known. For the internal bone anatomy, the compact part was represented by the P surface, since the pores are interconnected horizontally and vertically uniformly (also, its body centered cubic BCC crystal configuration allows to mimic the amorphous configuration of this bone section), with a porosity of $\approx 10\%$ and an average pore size of 0.100 mm. Then, the trabeculae were be represented with the G surface, which gradually increased its porosity from 60% to 90%, augmenting also the diameter from 0.500 mm to 1.2 mm.

III. Results

This part shows the results after applying the equations in the previous section. The design proposal for a bone scaffold is also presented. It is shown the comparison between using implicit and parametric equations, as well as the potential benefits of using the parametric methodology.

A. Parametric surfaces

Fig. 1 summarizes the process to obtain the complete parametric surface of each type (D, P and G). After the evaluation of (1) to (3), the FP was obtained, and then rotated following the symmetry operations until the complete CC was achieved. The normal vectors were computed and an offset value was calculated in order to vary the pore size.

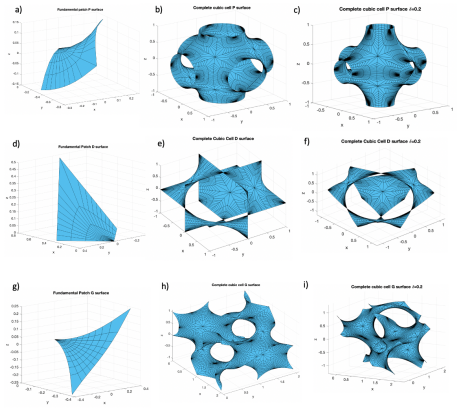

Fig. 1. Generation of the complete surfaces based on the fundamental patch.

a)-c) P surface. a)Fundamental patch (FP). b) Complete cubic cell (CC). c) CC pore size varied $\delta = 0.2$. **d)-f)** D surface. d) FP. e) CC. f) CC $\delta = 0.2$. **g)-i)** G surface g) FP. h) CC. i) CC $\delta = 0.2$

B. Porosity gradient

To control the pore size, the δ was characterized following the methodology aforementioned. The δ value was varied from -0.3 to 0.3 until self-intersections were observed. The pore/strut ratio ξ was measured along its diagonal, and a relationship between ξ and δ was obtained with a polynomial fit ($R = 0.9985$), resulting in (4):

$$\begin{aligned} \xi = 32589.24\delta^7 - 11034.59\delta^6 - 2691.78\delta^5 \\ -1272.23\delta^4 + 116.19\delta^3 - 18.13\delta^2 + 7.51\delta + 1.03 \end{aligned} \quad (4)$$

A relationship between porosity percentage n and a variation constant C [12], is established in (5):

$$C = 0.786n^3 - 1.179n^2 - 2.529n + 1.4597 \tag{5}$$

However, (5) considers a variation in the implicit geometry, with C from -1.5 to 1.5, therefore, it should be modified according to δ range of variation $\delta = \frac{C*0.3}{1.5}$. The relationship between pore size (dimensionless) and δ is in (6):

$$\begin{aligned} PoreSize = 563.61\delta^7 - 235.88\delta^6 - 16.13\delta^5 \\ +30.09\delta^4 - 0.29\delta^3 - 0.03\delta^2 - 1.69\delta + 0.44 \end{aligned} \tag{6}$$

In this way, the coordinates can be adapted to the actual pore sized desired by dividing it over the pore size obtained with (6).

The design for a bone scaffold proposed in this work, as described in the previous section, is depicted in Fig.2 and 3.

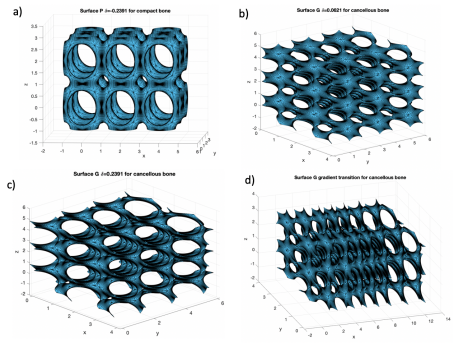

Fig. 2. Bone scaffold design with porosity gradient along x-axis. a) Surface P, pore size of 0.10 mm and $n = 10\%$. b) Surface G $n = 60\%$, pore size 0.50 mm. c) Surface G, $n = 90\%$, pore size 1.2 mm. d) Complete gradient of the G part, with intermediate pore size to make a smooth transition.

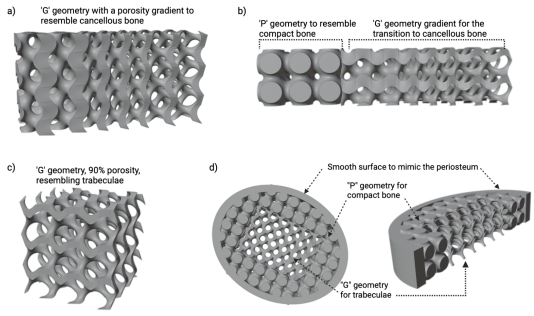

Fig. 3. Solid designs to resemble the bone micro-architecture. Created in MATLAB 2019a ® and rendered with Blender ®. a) G porosity gradient. b) Scaffold showing the transition and hybridization between the P and G geometries. c) G scaffold only for bone trabeculae. d) Scaffold to resemble an oval section of the distal metaphysis of long bones.

C. Geometry analysis

With the parametric approach, exact TPMS were obtained, preserving H=0 and K< 0. In Fig. 4, its difference against implicit approximation is clear; in the implicit, as the pore size varied, its shape changes by edge sharpening, which will influence the cells behavior, since, when cells are subjected to non-circular channels, the growth is slow, and there is risk of detachment [5]. The H was computed for both surfaces, resulting in 0 for the parametric, and 3.3077^{-6} for the implicit, which although is small, is not 0, as should be for TPMS.

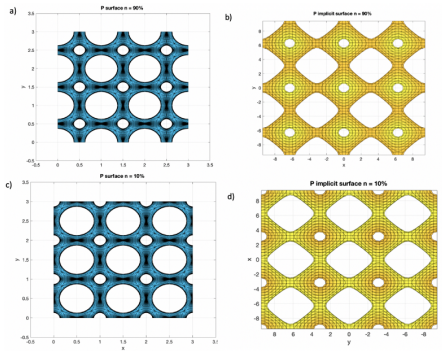

Fig. 4. Pore shape differences between P surfaces generated with the parametric approach versus the implicit equation [7]. a) P parametric $n = 90\%$, b) P implicit $n = 90\%$. c) P parametric $n = 10\%$. d) P implicit $n = 10\%$.

Another benefit of a parametric structure based on a FP is that it allows the analysis of some of its properties in a simple way without having to study the entire scaffold, thanks to the periodicity of the TPMS and the homogeneity that is gotten from the patch. For instance, continuing with the influence of curvature on cell behavior, Fig. 5 shows a diagram representing the points of cell adherence on the FP based on [1], [5]. A "chord analysis" can be performed on the FP considering that it will behaves as a saddle surface due to K< 0, moreover, the H=0 can decrease the risk of detaching.

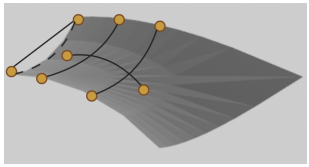

Fig. 5. FP curvature and a diagram of possible cell adhesion points. The points indicate less possibility of cell detaching and no nucleus stress due to stretching or compressing on cylindrical surfaces for example.

Mechanical stress simulations can also be performed on the FP, as presented in Fig. 6, where is shown an example of a Finite Element Analysis for displacement, done on a FP and CC of P type, with a Young modulus of 34.3 kPa (considering *GelMa* hydrogel [13]), a Poisson ratio of 0.167 and a vertical force of 1 MPa applied on the superior faces [3]. The analysis on the FP can be useful to determine exact zones of displacements. The time used to compute the simulation in the FP was two times less than in the CC.

D. Applications

To make this work useful to design diverse tissue scaffolds, a graphical user interface was implemented (Fig. 7). It will only need a few inputs, like TPMS type, pore size and gradient direction. It will do all calculations according to the previous methodology, ending with the solid file, ready

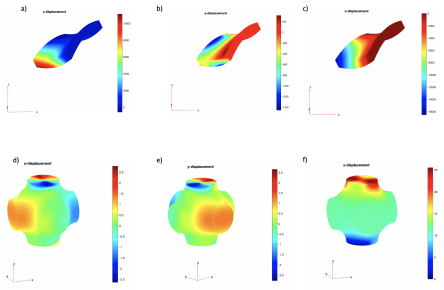

Fig. 6. Finite element analysis example for a P parametric structure

for additive manufacturing, as presented in the examples of Fig. 8.

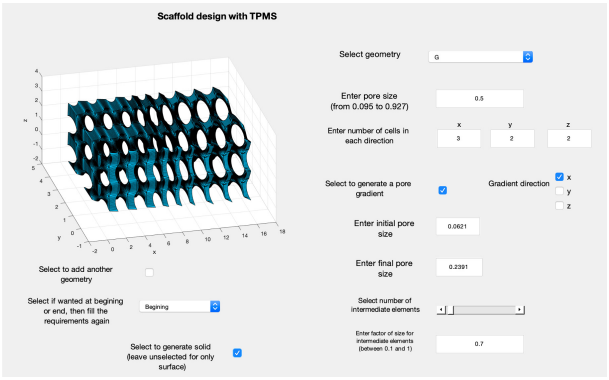

Fig. 7. Graphic user interface to generate distinct scaffold geometries.

.

IV. Discussions

A new methodology was proposed and implemented with the final goal of designing a bone porous scaffold using TPMS modeled with parametric equations. The above results, showed that a parametric mesh can be obtained by solving the Weierstrass equations, resulting in exact representation of these surfaces, respecting their minimal curvature that otherwise will be lost (with implicit equations). This curvature preservation is a potential benefit for cell growth and adherence. One of the major added value is the pore size variation of the surfaces in the parametric space, allowing continuous transitions and the possibility to represent different parts of the bone architecture. This aspect, along with the curvature, are what make the scaffold to be biomimetic. Moreover, this design procedure allows the exportation of solid files which can be directly 3D printed. This methodology possess a new option for modeling cell growth in distinct scaffolds, since it can be analyzed from a FP. This can suggest that parametric TPMS have potential to be used to mimic different anatomical shapes, enabling even the combination with patient-specific data. Therefore a graphical interface is proposed for the design of scaffolds not only for bone, but for different tissues.

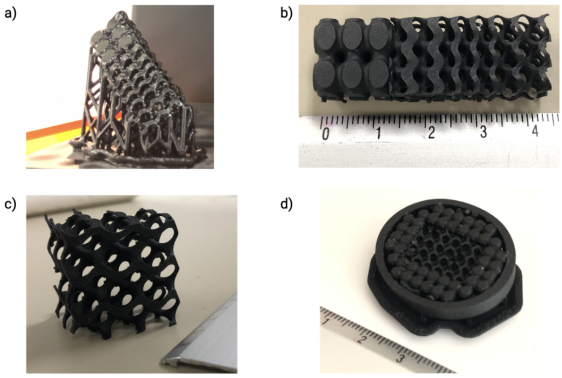

Fig. 8. 3D printed structures. a) Stereolitography process to obtain the structures, using black resin and a Form 2®printer [15]. b) Transition between P $n = 10\%$ and a G gradient (60 - 90 %). c) G structure $n = 90\%$. c) P and G structure enclosed in an oval shape.

Acknowledgment

M.F. acknowledges a Ph.D. stipend from CONACYT and a tuition scholarship from Tecnológico de Monterrey. R.F. acknowledge support from the School of Engineering and Sciences at Tecnológico de Monterrey.

References

[1] Bidan, C., Kollmannsberger, P., Kommareddy, K., & Brechet, Y. (2012). How Linear Tension Converts to Curvature: Geometric Control of Bone Tissue Growth. PLoS ONE 7(5).

[2] Bobbert, F., & Zadpoor, A. (2017). Effects of bone substitute architecture and surface properties on cell response, angiogenesis and structure of new bone. Journals of Materials Chemistry, 5, 6175-6192.

[3] Boccaccio, A., Uva, A., Fiorentino, M., Mori, G., & Monno, G. (2016). Geometry Design Optimization of Functionally Graded Scaffolds for Bone Tissue Engineering: A Mechanobiological Approach. PLoS ONE, 11(1).

[4] Bose, S., Vahabzadeh, S., & Bandyopadhyay, A. (2013). Bone tissue engineering using 3D printing. Materials Today, 16(12).

[5] Callens, S., Uyttendaele, R., Fratilaa-Apachitei, L., & Zadpoor, A. (2020). Substrate curvature as a cue to guide spatiotemporal cell and tissue organization. Biomaterials, 232.

[6] Chen, X. (2019). Extrusion Bioprinting of Scaffolds for Tissue Engineering Applications. Springer Nature. ProQuest Ebook.

[7] Gandy, P., Bardhan, S., Mackay, A., & Klinowski, J. (2001). Nodal Surface approximations to the P, G, D and I-WP triply periodic minimal surfaces. Chemical Physics Letters, 336, 187-195.

[8] Gandy, P., Cvijovic, D., Mackay, A., & Klinowski, J. (1999). Exact computation of the triply periodic D ('Diamond') minimal surface. Chemical Physics Letters, 314(5-6), 543-551.

[9] Gandy, P., & Klinowski, J. (2000). Exact computation of the triply periodic G ('Gyroid') minimal surface. Chemical Physics Letters, 321(5-6), 363-371.

[10] Gandy, P., & Klinowski, J. (2000). Exact computation of the triply periodic Schwarz P minimal surface. Chemical Physics Letters, 322(6).

[11] Melchels, F., Bertoldi, K., Gabbrielli, R., Velders, A., Feijen, J., & Grijpma, D. (2010). Mathematically defined tissue engineering scaffold architectures prepared by stereolithography. Biomaterials, 31, 6909-6916.

[12] Walker, J., Bodamer, E., Kleinfehn, A., Luo, Y., Becker, M., & Dean, D. (2017). Design and mechanical characterization of solid and highly porous 3D printed poly(propylene fumarate) scaffolds. Progress in Additive Manufacturing, 2, 99-108.

[13] Wu, Y., Xiang, Y. & Zhang, D. (2019). The influence of the stiffnes of GelMA substrate on the outgrowth of PC12 cells. Bioscience Reports (39)1.

[14] Zadpoor, A. (2014). Bone tissue regeneration: the role of scaffold geometry. Biomaterials Science. Royal Society of Chemistry.

[15] Formlabs 2021. Recover from https://formlabs.com